Wind and Structures, Vol. 6, No. 5 (2003) 403-418
DOI: http://dx.doi.org/10.12989/was.2003.6.5.403

Short term unsteady wind loading on a low-rise building

M. Sterling† and C.J. Baker‡

School of Engineering, The University of Birmingham, Edgbaston, Birmingham, B15 2TT, UK

R.P. Hoxey‡†

Silsoe Research Institute, Wrest Park, Silsoe, Bedford, MK45 4HS, UK

(Received August 9, 2003, Accepted October 17, 2003)

Abstract. This paper presents an extensive analysis of the short term, unsteady wind loading on a low-rise building. The building is located in a rural environment and only the specific situation of wind flow orthogonal to the long face of the structure is considered. The data is analysed using conventional analysis and less traditional methods such as conditional sampling and wavelet analysis. The nature of the flow field over the building is found to be highly unsteady and complex. Fluctuating pressures on the windward wall are shown to a large extent to be caused by the fluctuations in the upstream flow, whereas extreme pressures on the roof are as a result of high intensity small scale flow structures. On the roof of the building a significant amount of energy is shown to exist at frequencies above 1 Hz.

Keywords: unsteady loading; conditional sampling; wavlet analysis; low-rise building.

1. Introduction

Over the last few decades a significant corpus of research has been amassed regarding the wind effects on high-rise structures. Research in this area is still ongoing and has yielded some interesting and important discoveries for structural engineers. Surprisingly, despite their common occurrence there has been less work undertaken to quantify the wind induced forces on low-rise buildings. Due to their interaction with surrounding structures and the corresponding wake effects that inevitably arise, low-rise structures can offer a degree of complication that does not exist in the analysis of their high-rise counterparts. Problems are further compounded by the lack of knowledge regarding the actual flow structures that exist in the lower region of the atmospheric boundary layer and also by the increased levels of turbulence found close to the ground.

In order to obtain structural loads it is not uncommon to consider the effect of a *t* second gust (ENV-1991-2-4, (CEN 1994); AS1170.2, (Standards Australia 1989)). This method effectively places a restriction on the size of the flow structures present in the wind that load the building. While such a restriction is acceptable for obtaining overall structural loads, pressure tappings located on cladding elements have shown that a significant amount of energy exists at high

† Lecturer
‡ Professor
‡† Head of Environmental Group

frequencies (Kho 2002, Kho, *et al.* 2002). This is not only of scientific interest, but raises important questions regarding possible fatigue effects on cladding elements, which at present are not taken into account in a structural design of a low-rise building.

In the UK, the vast majority of structures are low-rise, and as such warrant in depth investigations. In this paper the unsteady short term wind loading on a low-rise building will be investigated using traditional and non traditional analysis. It will be shown that despite the simple geometry of the low-rise building the unsteady flow field is complex. The experimental details are presented in section 2, while section 3 examines the results of an analysis using conventional methods e.g., moments of probability distributions and power spectra. Conditional sampling is used in section 4, while section 5 is concerned with the application of wavelet analysis. The final part of the paper, section 6, presents some concluding remarks based on the findings of the research.

2. Experimental data

The Silsoe Structures Building (SSB) has been fully described elsewhere (Hoxey, *et al.* 1995, Prevezer 1998) and as such only brief details relevant to this experimental data are presented here. The building is 4 m high to the eaves, 24 wide and 12 m deep with a roof slope of 10 degrees (Fig. 1). It has two basic configurations - with either sharp or curved eaves. In what follows attention will be restricted to analysing results for the centreline of the building with the wind approximately 90^o to the long face, for the sharp eaves case only. The SSB is located in open country with a logarithmic velocity profile with a roughness length (z_o) of around 0.01 m and a power law exponent of 0.15 (Richardson, *et al.* 1995). Further details of the spectral characteristics of the flow are given in Richards, *et al*. (1997). Four specific datasets were obtained for the flow approximately normal to the building on 16th October 1991. These datasets were obtained from 1 hours worth of recording and represent four 15 minutes worth of consecutive data. The results that follow are presented for all datasets and show that the main statistical moments for all the data (means, standard deviations, skewness etc.) and spectral characteristics are similar.

All four data sets are each approximately 13 minutes in length and were obtained at a sampling rate of 20.8 Hz (i.e., each dataset contains 16384 data points for each velocity component and pressure tapping). The wind characteristics were measured using a sonic anemometer and static

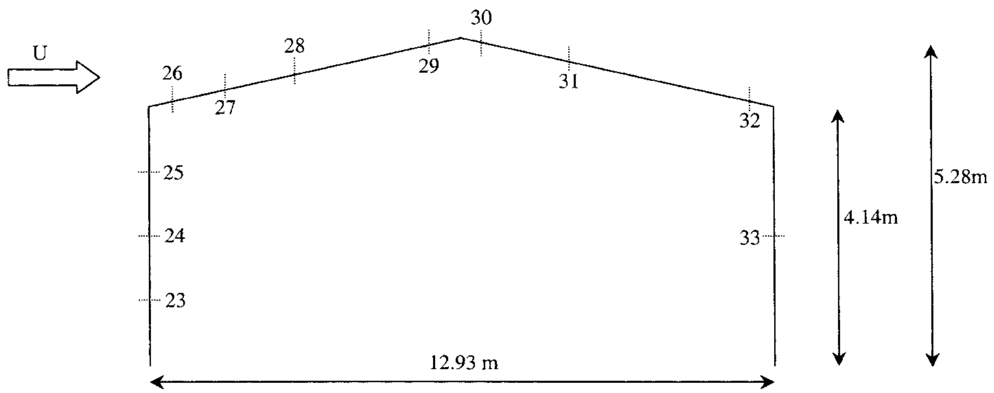

Fig. 1 The Silsoe Structures Building. Dashed lines and numbers 23−33 represent pressure tappings

Table 1 Conventional statistical analysis of experimental data

Parameter	Dataset 1	Dataset 2	Dataset 3	Dataset 4	Average	Standard deviation
U (ms^{-1})	8.200	7.960	8.294	8.619	8.268	0.273
σ_u/U	0.220	0.216	0.288	0.283	0.252	0.039
σ_v/U	0.192	0.170	0.244	0.289	0.224	0.053
σ_w/U	0.084	0.077	0.089	0.091	0.085	0.006
s_u	-0.847	0.147	-0.111	-0.192	-0.251	0.423
s_v	-0.651	-0.432	-0.519	-0.639	-0.560	0.104
s_w	0.062	0.179	-0.266	0.027	0.010	0.171
s_q	-0.032	0.743	0.567	0.539	0.454	0.697
U_e/U	1.521	1.650	1.740	1.817	1.682	0.127
u_{max}/U	1.587	1.784	1.789	1.976	1.784	0.159
u_τ/U	0.059	0.053	0.046	0.047	0.051	0.006

pressure probe mounted at ridge height, 20 m upwind of the SSB. Table 1 illustrates the experimental conditions pertinent to the data analysed in this paper.

Table 1 gives the mean wind speed U, the three turbulence intensity components σ_u/U, σ_v/U and σ_w/U, the skewness of the three velocity components s_u, s_v and s_w, the skewness of the dynamic pressure, s_q, and the ratio of the extreme wind speed to the mean wind speed, U_e/U. This extreme wind speed is the 99.95th percentile and corresponds to 0.4 seconds of the dataset. u_{max} is the maximum recorded velocity obtained in each of the datasets and the dimensionless friction velocity is represented by u_τ/U. The u component is parallel to the mean flow direction, the v component is horizontal and perpendicular to the mean flow direction, and the w component is in the vertical direction. The final two columns of Table 1 represent the mean and standard deviation of specific parameters across all four datasets.

At first glance the results obtained appear to be reasonably consistent, for example there is a maximum difference of 8.3% in terms of U. The lateral values of skewness are of similar order of magnitude for all the data collected, however there are inconsistencies in signs in both the longitudinal and vertical values. The skewness of the dynamic pressure is interesting since it highlights an apparent anomaly in sign and magnitude between dataset 1 and the other datasets. The dynamic pressure statistics are encouragingly similar between the remaining datasets, with a surprisingly close agreement between datasets 3 and 4. The values of mean velocity, friction velocity and turbulence intensities for all three velocity components are consistent with values that would be expected over rural terrain (ESDU 1985). The ratio of maximum to mean velocity is of the order of 1.7 and is perhaps somewhat lower than that would have been expected. For example, Baker (2001) obtained values of the order of 2.0 for the same experimental site, however, it should be noted that in that analysis the flow had a mean velocity of the order of 10 ms^{-1} and a corresponding value of σ_u/U of 24%. Obtaining consistent data in full-scale conditions is difficult since the velocity can rarely be considered to be truly stationary. The mean and standard deviations in Table 1 illustrate that the data are reasonably consistent and suggests some degree of stationarity. However, the higher order skewness statistics show a large degree of variability. Notwithstanding this issue, the data is broadly consistent and of similar magnitudes to enable detailed analysis to be

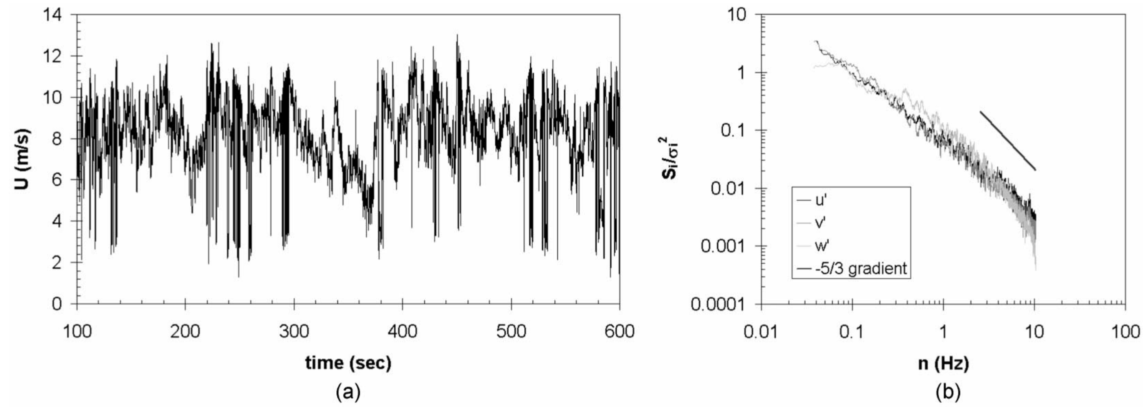

Fig. 2 (a) Snapshot of the velocity time series for dataset 1; (b) Veloicty power spectra for dataset 1

undertaken with confidence in the applicability of the results.

A typical u velocity time series is shown in Fig. 2(a). Perhaps the most noticeable features are the discrete short duration "spikes" in the time series associated with the extreme events. This results in a non-zero skewness for this velocity component (–0.847, Table 1) and also for the v component. Fig. 2(b) illustrates the power spectra for all three velocity components. The spectral density for each component (S_u, S_v, S_w) is divided by its variance (σ_u^2, σ_v^2, σ_w^2) and plotted against frequency n. The inertial sub range is clearly seen at higher frequencies for all three components, i.e. the slope of the curves are close to the expected (–5/3) value as illustrated in Fig. 2(b). This is consistent with the results of Baker (2001) and Richards, *et al.* (1997) who both analysed data from the same experiment site.

In the analysis that follows the results are presented for 11 pressure tappings. Tappings 23, 24 and 25 are on the windward side of the building, 26–29 on the windward side of the roof, 30–32 are on the leeward side of the roof and tapping 33 on the leeward wall (Fig. 1). In what follows it will be demonstrated that the separation zone on the roof is highly unsteady, however for the majority of the time, tappings 26, 27 and 28 are within this zone. The pressures were sampled at 20.8 Hz, with the static reference from a probe at the anemometer position.

3. Analysis via conventional methods

Instantaneous pressure coefficients, defined by Eq. (1) where p is the instantaneous surface pressure, p_r is the instantaneous reference pressure, ρ is the density of air and u is the instantaneous velocity, were calculated. Using this data mean, standard deviation and skewness values were obtained for each pressure tapping (Fig. 3).

$$C_p = \frac{p - p_r}{0.5\,\overline{\rho u^2}} \tag{1}$$

The mean coefficients on the windward wall (tappings 23, 24 and 25) are all positive and reasonably uniform when compared to the majority of the mean coefficients over the roof, as

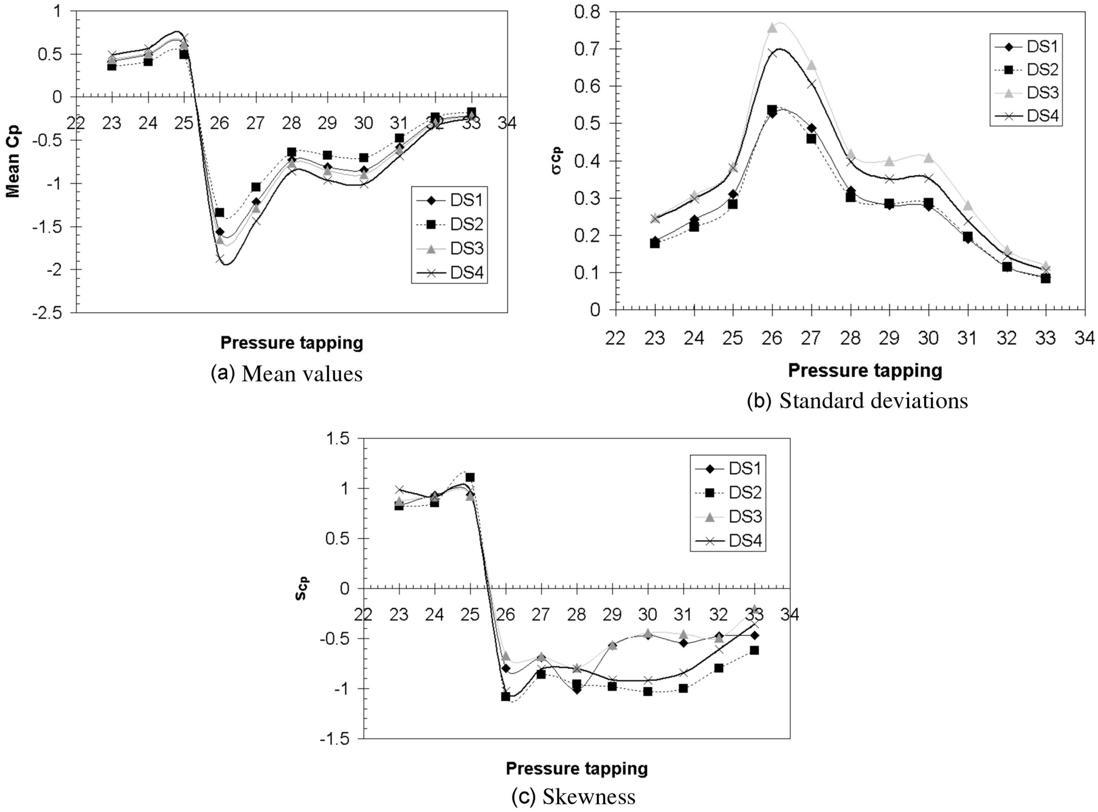

Fig. 3 Characteristics of pressure coefficients. Dsi, where i=1 to 4 indicates the relevant dataset

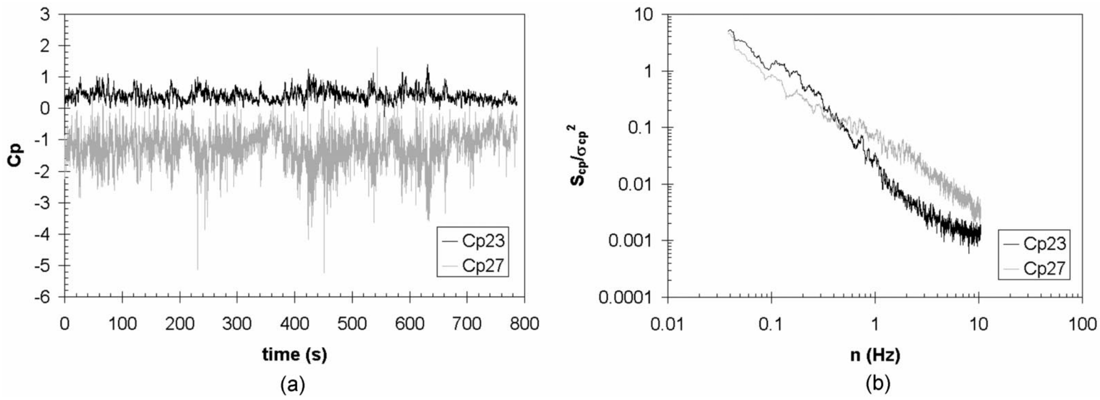

Fig. 4 Typical time histories and corresponding spectra for two pressure tappings on the windward side of the building [Cp23 windward wall, Cp27 windward roof]. Dataset 1

evident from Fig. 3(a). The mean value of C_p over the roof and leeward wall are all negative and demonstrate no unexpected behaviour. The standard deviations of the pressure coefficients (σ_{Cp}) in Fig. 3(b) broadly reflect the mean pressure distributions, with the highest values occurring at the leading edge of the windward roof. The flow separation at the leading edge of the windward roof (tapping 26) is evident by the large negative value of pressure coefficient at this point. The corresponding value of standard deviation also suggests that the region of separated flow is highly unsteady and in some instances can extend to tapping 28, i.e., a distance of approximately 3.5 m. The skewness values of pressure coefficient (s_{Cp}) depart significantly from zero with magnitudes of unity in some cases (Fig. 3(c)). An analysis of the individual time series of pressure coefficients (Fig. 4(a)) illustrates that the large coefficients are associated with relatively short duration peaks of an intermittent nature and it is these peaks which lead to the large values of skewness. These peaks are similar to some degree to the peaks in the upwind dynamic pressure time series and the values of skewness on the windward wall are of the same magnitude to those of the dynamic pressure given in Table 1.

Fig. 4(b) illustrates the spectra for the two pressure coefficient time series. The time series for the pressure tapping situated on the windward roof (tapping 27) contains more energy at frequencies

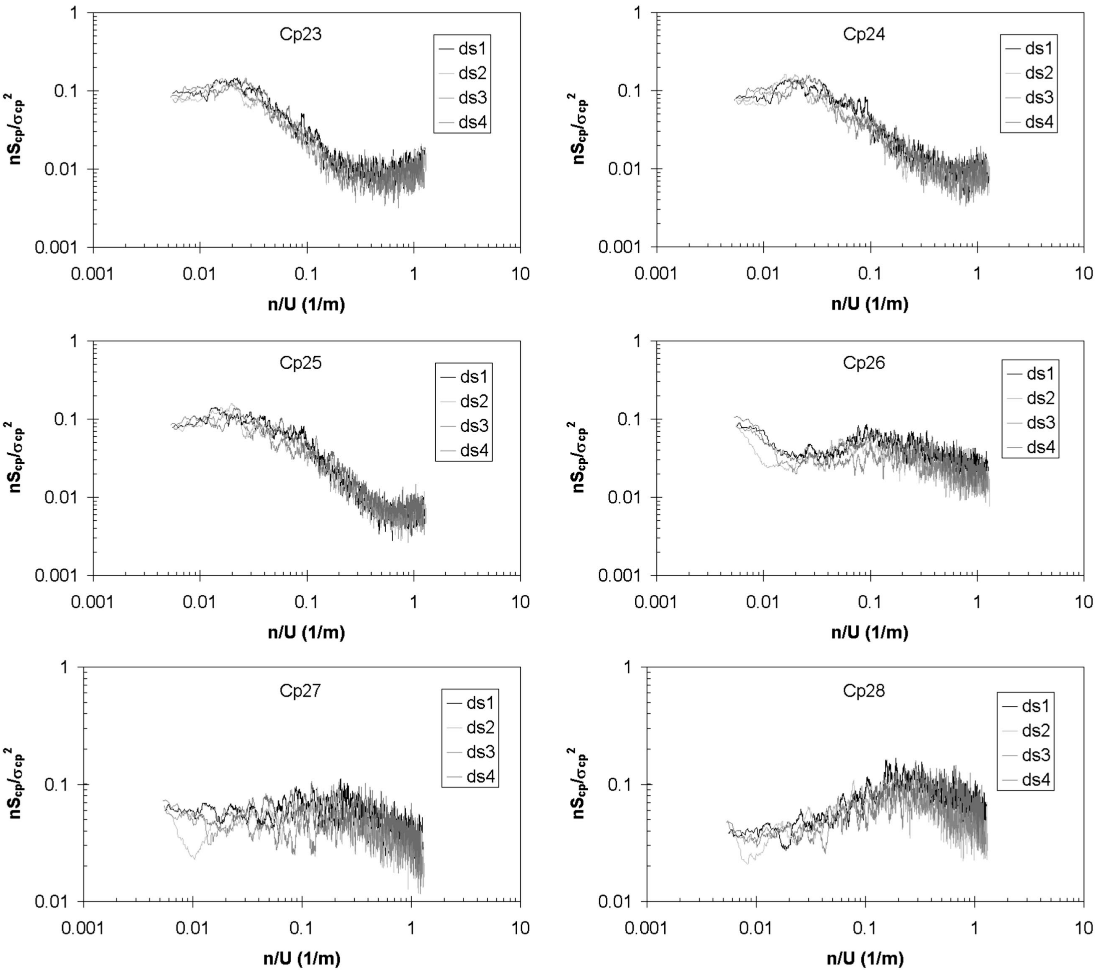

Fig. 5 Spectral plot for pressure tappings around the building for all datasets

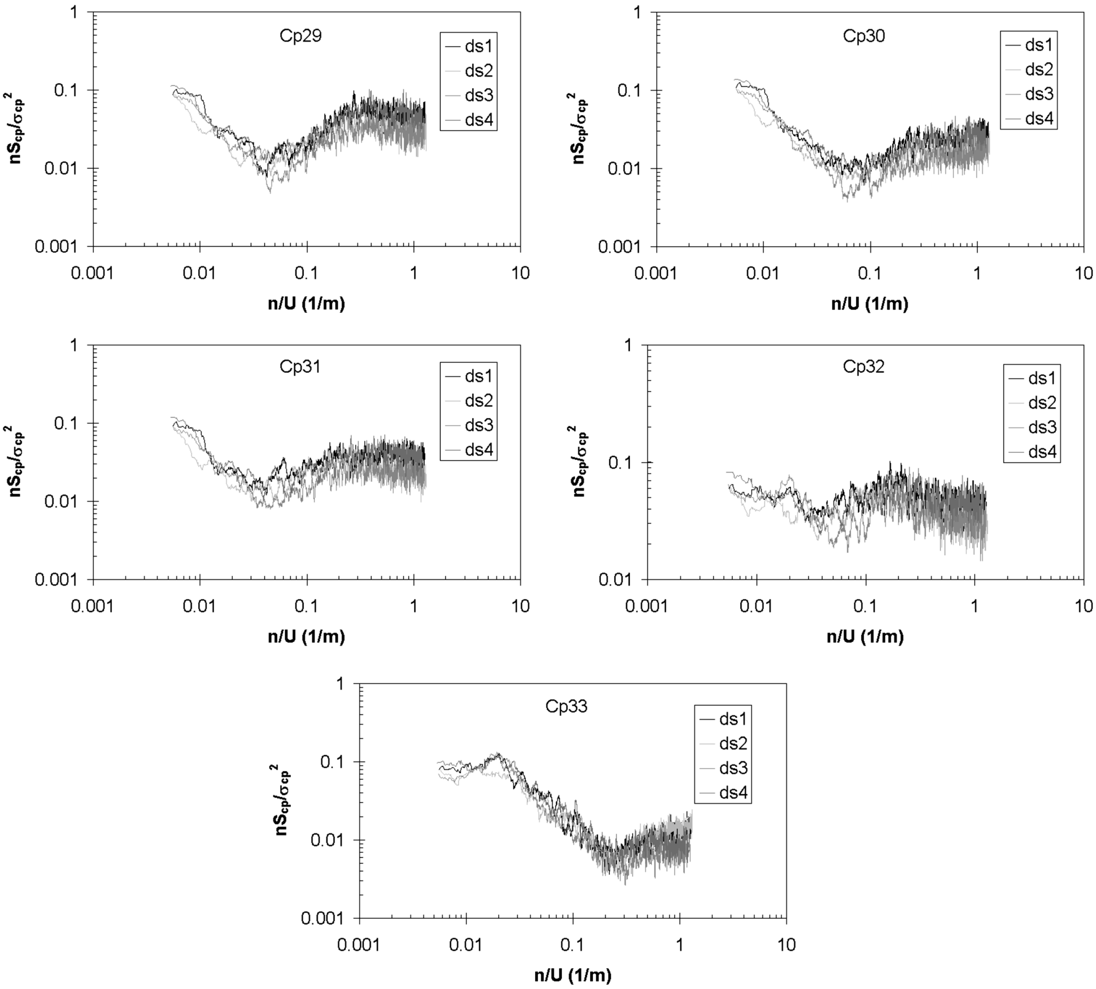

Fig. 5 Continued

above 0.8 Hz, than a corresponding tapping situated on the windward wall (tapping 23). This illustrates that there is a large amount of energy associated with high frequency, short term fluctuations and again supports the conjecture presented above regarding the length of the region of flow separation. These findings are supported by the work of Letchford, *et al.* (1993) who also discovered that at higher frequencies the pressure spectra on the roof of the Texas Tech Building are under estimated by the quasi-steady theory. Letchford, *et al.* state that this underestimation is due to an increase in energy associated with wake turbulence, which in the case of tapping 27 would be as a result of the separation zone.

A complete set of spectral plots for the whole structure are shown in Fig. 5. The spectra have been plotted in nS_{cp}/σ_{cp}^2 form to enable a direct comparison of the energy contained in each of the time signals. The horizontal axis of Fig. 5 is expressed in terms of n/U in an attempt to reduce the effect of the difference in mean velocity and enable comparison. Fig. 5 clearly illustrates that for each individual pressure tapping there is little discernable difference between the shapes of the curves for each dataset. This is encouraging and again highlights the overall apparent consistencies in the datasets. At this stage it is worth mentioning that the data in Fig. 5 have been analysed from the raw collected data, i.e., no filtering has been applied prior to the signal processing, and thus we may expect a degree of aliasing at the higher frequencies.

The spectra in Fig. 5 illustrate some interesting results and highlight how the distributions of energy within the pressure tappings vary around the structure. For example, considering the windward wall data (Cp23-Cp25) it is evident that the peak in the signal occurs around a value of n/U equal to 0.02 (approximately 0.2 Hz), while the lowest value occurs in the high frequency range of the signal, i.e., n/U~0.7 (~5 Hz). The situation on the windward roof (Cp26-Cp29) is significantly different, with the peak in the signal occurring at increasing frequencies (0.8 Hz−5 Hz; n/U~0.2 to 0.8) as the distance from the leading edge of the roof increases. These results give credence to the statement made earlier that Cp28 is within the separation zone. The information presented in Fig. 5 suggests that the flow within this zone is dominated by high frequency, small-scale flow structures.

The spectra for the leeward roof follow similar trends and show a relatively constant reduction in energy up to values of n/U equal to 0.06, with a constant trend across the higher frequencies. The trend for the leeward wall (Cp33) is similar to those of the windward wall, i.e., a sharp decrease in energy from n/U~0.02 to n/U~0.2. This is surprising since the flow immediately in the lee of the building is dominated by building induced turbulence, whereas the flow on the windward wall is not. A possible explanation for the high energy values at high frequencies may be attributed to a slight increase in the degree of aliasing of the pressure signals, however this would not explain the high energy, high frequency behaviour which is presented in the next section.

Fig. 6 shows the distribution of extreme values of pressure coefficient (C_{pe}) corresponding to the 99.95th percentile. The distribution follows the same pattern as mean values and highlights the very high suction values at the leading edge of the windward roof. These extreme values represent gust factors (defined as (extreme−mean)/standard deviation) of approximately four over a large proportion of the structure, i.e., in excess of values expected for a Gaussian process (i.e., 3 to 3.5). This simplified approach to determining the gust factor whilst open to debate is, however, adequate for illustrative purposes.

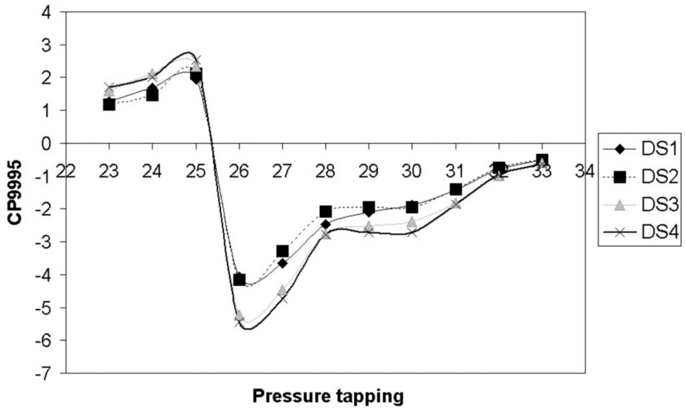

Fig. 6. Extreme values of pressure coefficient

4. Analysis via conditional sampling

Similar to the findings obtained by Baker (2001), it is evident from the above that the extreme loads on the roof are to some extent due to discrete high frequency events. In order to investigate this further a conditional sampling technique has been employed similar to that adopted by Letchford and Mehta (1993), Kareem (1997) and Baker (2001). Firstly discrete events were identified at a particular pressure tapping. These were defined as when the pressure coefficient exceeded the 99.95th percentile value. “Events” less than two seconds apart were taken to be one event with the peak value being given by the greater peak. During each event the time at which the maximum value occurred was noted. Table 2 illustrates the number of events identified at each pressure tapping for each dataset.

At this stage it is worth noting that the number of events identified at each tapping, for each dataset are reassuringly consistent. There is a significant increase in the number of events on the windward roof compared to the windward wall, with the maximum number of single events occurring at Cp28. This is not too surprising since this particular pressure tapping is at the edge of a highly unsteady region of separated flow. Hence, the constant attachment/separation of the shear layer will inevitably produce a relatively large increase in values of pressure coefficients leading to more events.

In order to analyse these events in more detail the pressure coefficients at a particular “trigger” (C_{pcs}) were examined as follows. Once the time at which a discrete event occurred was identified, the surrounding values of pressure coefficients for 4.5 seconds either side of the event were noted and used to produce a mini time series of 9 seconds worth of data zeroed on the actual event. An average across all of the datasets was then produced for each individual time step. The results of this process are illustrated in Fig. 7, where Cp24 has been taken as the trigger and expressed as a ratio of C_{pcs} divided by the mean value C_p at each pressure tapping.

Fig. 7 illustrates that an event occurring on the windward face of the SSB is not well correlated with the pressure distribution over the rest of the structure, as evident by the relatively flat distributions for Cp26−Cp33. A closer inspection of the time series for Cp28 identifies a sharp decrease followed by an immediate increase in pressure coefficient a fraction of a second after the

Table 2 Number of extreme events occurring at each pressure tapping (DS = dataset)

Tapping	DS1	DS2	DS3	DS4	Total
23	1	2	2	1	6
24	2	1	2	3	8
25	3	1	2	2	8
26	5	5	3	6	19
27	5	4	3	5	17
28	5	7	6	7	25
29	6	4	6	6	22
30	5	3	3	3	14
31	6	3	4	6	19
32	7	4	5	5	22
33	4	1	0	1	6

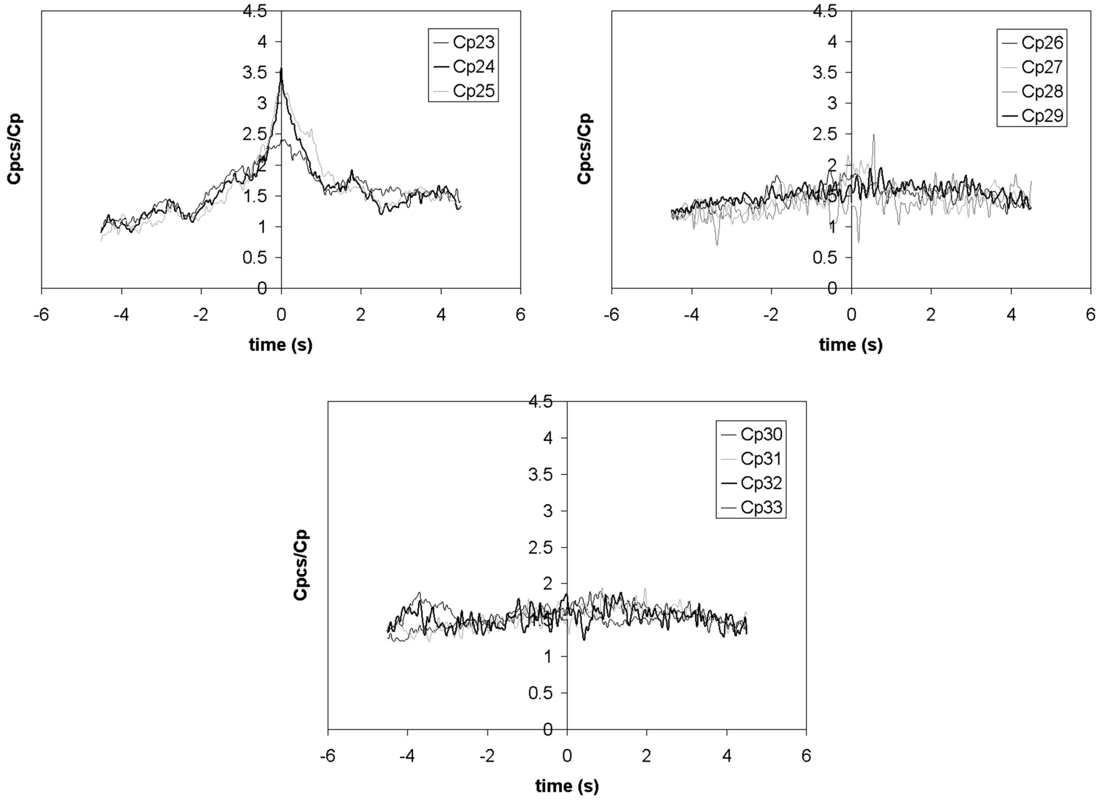

Fig. 7 Conditional sampling, Cp24 used as a trigger

identification of the event. However, since this trend is an average of only 8 events care must be exercised in this interpretation. There is evidence however to suggest that events on the front face of the building are reasonably well correlated with each other and extend over an approximately one second time period. The maximum average values of the events are in the region of 3.5 which is consistent with what would be expected of a Gaussian distribution. It is interesting to note that for all pressure tappings the underlying value of pressure coefficient is at least 50% greater than the mean value over the 9 second event time, suggesting that the extreme events are relatively small in physical size and embedded in larger flow structures which envelope the SSB.

Fig. 8 illustrates a similar analysis but uses Cp28 as a trigger. Again there is strong evidence to suggest that the pressure coefficient values on the windward wall are reasonably well correlated with each other but not with the rest of the structure. There is a slight increase on the windward wall suggesting a possible weak correlation with the event at Cp28. The tappings on the leeward roof and wall show no indication that an event on the windward roof has occurred. The reason for this lack of detection is evident after consideration of the time history for Cp28; a high intensity, short duration event occurs and on average lasts for approximately 0.1 seconds. There is no indication in any of the pressure tappings on the windward roof that this event has occurred, suggesting that the horizontal component of such an event is small and that the main motion is

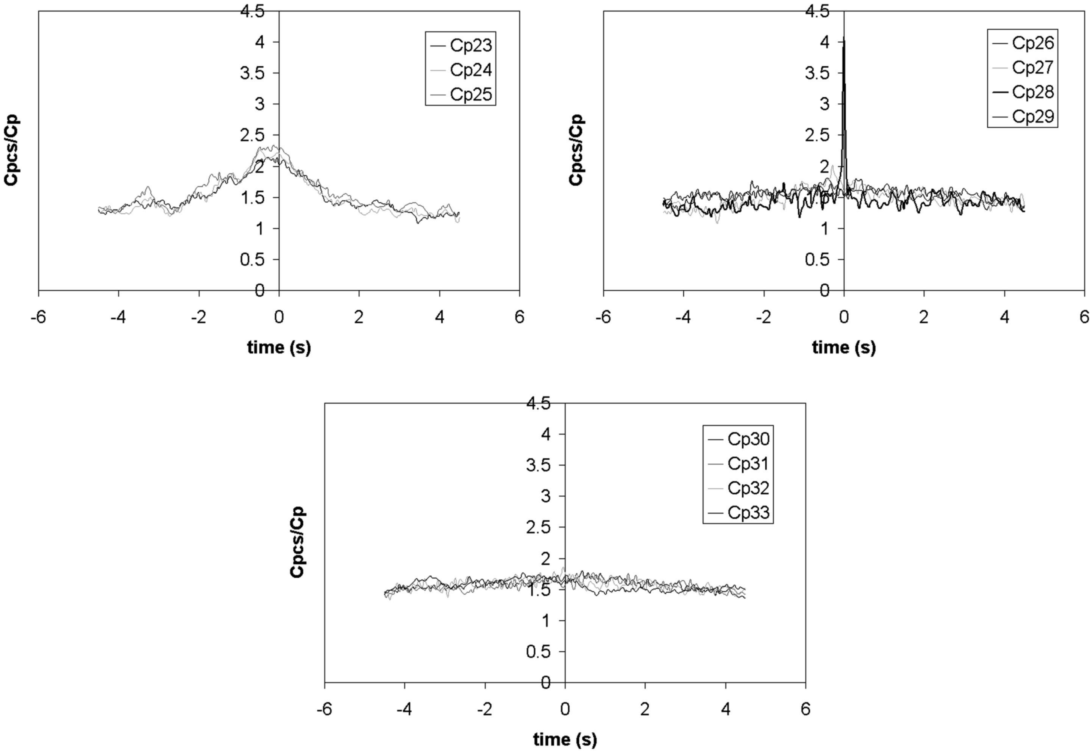

Fig. 8 Conditional sampling, Cp28 used as a trigger

vertically downwards. Similar results (not shown) have been obtained for triggers at Cp27 and Cp32. The main difference between these results and those of Cp28 are the maximum value of C_{pcs}/C_p, which is 3.5 for Cp27 and Cp32 as opposed to 4.0 for Cp28.

By their very nature conditional sampling techniques are subjective since a lower threshold criteria could have been adopted and consequently more events detected. Despite this, the brief analysis presented above illustrates that the loading of the SSB is indeed dominated by intermittent, discrete events with varying time scales. There is evidence to suggest that small scale structures are superimposed on the larger scale events which envelope the SSB. Despite the size of these small scale structures and the corresponding lack of correlation between pressure tappings, it is evident from Fig. 8 that peaks in Cp28 do occur when there are medium sized peaks on the windward roof, suggesting that there may be some weak interaction. This may be further evidence of the unsteady nature of the separation zone.

The next section attempts to further explore the relationship between the spatial and temporal structure of these extreme events.

5. Wavelet analysis

The intermittent nature of the pressure coefficient time histories (Fig. 4) and their statistical characteristics (Fig. 3) provides striking evidence of the spatial and temporal variability inherent in

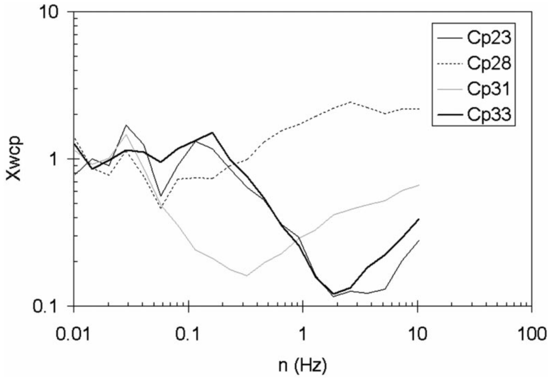

Fig. 9 Wavelet spectra admittances for selected pressure tapings

the wind loading of the SSB. This variability probably arises as a result of energy contained within the wind being organized into distinct coherent structures, as evident by the conditional sampling of section 4. In addition to the techniques employed above it is possible to examine this phenomena using wavelet mathematics.

The development of wavelet analysis has now reached a stage where it is possible to analyse the temporal variation of energy with frequency within a given signal. A good description of the use of wavelet analysis is given in Torrence and Compo (1998), and its application to wind engineering are discussed in Gurely and Kareem (1999). In the analysis that follows, the Morlet wavelet has been adopted:

$$\psi(\eta) = \pi^{-1/4} e^{i\omega_o \eta} e^{-\eta^2/2} \tag{2}$$

where η is a non-dimensional time period, ω_o is a non-dimensional frequency, here taken to be 6 (Farge 1992) and $i = \sqrt{-1}$. Twenty-one distinct scales or periods were used in the analysis and ranged from 0.096 secs to 98.304 secs. For each time series this resulted in a set of 21 time series of the same length across the range of periods. Fig. 9 shows the mean wavelet spectra ($W_{cp}(s)$) obtained from finding the average of each of these time series. The results are shown in an admittance form defined as:

$$X_{wcp} = \frac{W_{cp}(s)/\sigma_{cp}^2}{W_u(s)/\sigma_u^2} \tag{3}$$

where the subscript u indicates the wavelet spectrum and standard deviation of the upstream mean velocity. The x axis is shown in terms of a Fourier frequency rather than a scale for ease of comparison with other spectra. All of the pressure tappings show an increase in wavelet power for frequencies above 2 Hz. The trend for Cp23 and Cp28 remains reasonably constant across the lower part of the frequency range ($n < 0.2$ Hz) suggesting that the fluctuations in the pressure directly follow fluctuations in the upstream wind velocity, i.e., the quasi steady assumption.

For frequencies above 1 Hz, a significant amount of energy exists in the time series of all the

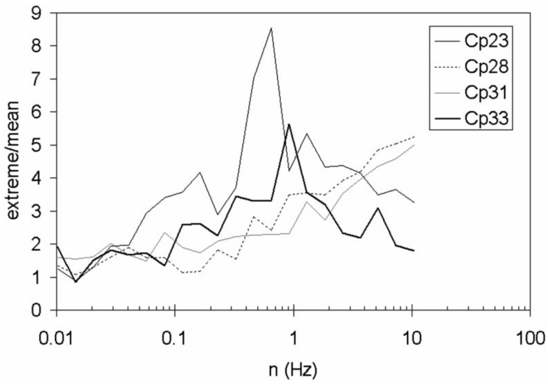

Fig. 10 The average ratio of extreme to mean wavelet power for Cp23

datasets of pressure tapping Cp28. This is significant since flow visualisation experiments have confirmed that the point of reattachment occurs close to the region of Cp28. The data presented in Fig. 9 broadly follows the average trend shown in 5, however it is interesting to note that for frequencies above 0.2 Hz the average fluctuations in the pressure do not appear to closely follow the average fluctuations in the wind velocity.

Fig. 10 shows the average wavelet power spectrum at each scale for a series of peak events identified using the conditional sampling of last section with the results for each pressure tapping averaged across all the datasets. The results are presented as a ratio of the extreme wavelet power spectrum (two second average) to the mean wavelet power spectrum. The data presented in these figures have been obtained by averaging the wavelet power across each frequency for all the events corresponding to a particular dataset (Table 2). Fig. 10 illustrates that the wavelet energy at the peak values occurs over a frequency range of 0.5−1 Hz across all of the datasets. Similar to the findings of Jordon, *et al*. (1997) and Baker (2001) it can be seen that on the roof of the SSB there is considerable enhancement of energy at higher frequencies (Figs. 11−12). This is particularly noticeable at frequencies above 1 Hz and may have implications on the design of structural cladding elements where the energy content at high frequencies is usually considered as negligible.

6. Discussion and conclusions

The flow around the SSB has been shown to be highly unsteady and intermittent in nature. Results obtained from conventional analysis suggests that the nature of the flow leads to structural loading which cannot accurately be represented by a Gaussian process. The large values of standard deviation calculated at the leading edge of the windward roof are indicative of an unsteady zone of separation. A visual inspection of the velocity time series, in addition to any of the pressure coefficient time series indicates the presence of short term sharp spikes. Fig. 4(a) illustrates that although the mean pressure coefficient on the leeward roof is predominately negative, constant positive pressures can occur for short periods of time. Figs. 4(b) and 5 highlight how the average distribution of energy with respect to frequency varies around the structure. This is important particularly in the separation zone and has implications in terms of structural design.

Conditional sampling of the pressure coefficients has confirmed the existence of high energy events which occur over a short time period. Events on the windward wall of the building have been shown on average to be reasonably well correlated with each other. There is little evidence to suggest that small scale events occurring on the windward wall are on average transported around the structure by the mean flow. However, a number of peaks in the conditional sampling of Cp28 do appear to be weakly correlated with peaks on the windward wall. Conditional analysis on the windward roof has also illustrated that on average the events are small scale but high intensity. The lack of detection of these events at other pressure tappings suggests that the vertical velocity component is relatively large compared with the horizontal, thus ensuring that the energy contained in these structures are dissipated over small areas. The data in Figs. 7 and 8 clearly illustrate that for a particular event the values of the pressure coefficients over the entire SSB take values which are on average 50% greater than the long term values. This suggests that the small scale events are superimposed on larger, less intense events which engulf the entire SSB.

Wavelet analysis has also highlighted the important role that extreme events have on the loading of the SSB. For extreme events a significant amount of energy is contained at frequencies above 1 Hz, i.e., frequencies that are often neglected in structural design. Fluctuating pressures on the windward wall are to a large extent caused by the fluctuations in the upstream flow and therefore reflect the oncoming flow structures. The fluctuating pressures on the rest of the structure are highly unsteady. In addition to being influenced by the fluctuations in the upstream flow, they are largely affected by the separation and corresponding wake flow. A significant amount of fluctuating energy is also apparent at high frequencies. It has been hypothesised that there is evidence to suggest the existence of small scale vortices embedded within large scale structures.

Despite the relative simple geometry of the SSB, the flow field over the building is highly unsteady and complex. Given this complexity and the importance of discrete structures evident from the pressure coefficient time series, it is highly unlikely that current quasi-steady methods used for load prediction would satisfactory represent the true forces imposed on the cladding elements of the SSB.

Notation

C_p	Pressure coefficient
C_{pcs}	Conditionally sampled pressure coefficient
n	Frequency (Hz)
p	Pressure (Nm^{-2})
p_e	Extreme value of pressure (Nm^{-2})
p_r	Reference pressure (Nm^{-2})
s_{cp}	Skewness of pressure coefficient
s_q	Skewness of dynamic pressure
s_u, s_v, s_w	Skewness of velocity components
S_{cp}	Spectral density of pressure coefficient
S_u, S_v, S_w	Spectral density of velocity components
t	Time (s)
u	Longitudinal velocity component (ms^{-1})
U	Mean reference velocity (ms^{-1})
u_τ	Friction velocity (ms^{-1})
v	Lateral velocity component (ms^{-1})
w	Vertical velocity component (ms^{-1})

$W_{cp}(s)$	Average value of wavelet spectrum
X_{cp}	Pressure coefficient admittance
X_{WCp}	Pressure coefficient wavelet spectrum admittance
σ_{Cp}	Standard deviation of pressure coefficient
σ_u, σ_v, σ_w	Standard deviation of velocity components (ms^{-1})
ψ	Wavelet function
ω_o	Non-dimensional wavelet frequency

References

Baker, C.J. (2000), "Aspects of the use of proper orthogonal decomposition in the analysis of surface pressure fields", *Wind Struct., An Int. J.*, **3**(2), 97-115.

Baker, C.J. (2001), "Unsteady wind loading on a wall", *Wind Struct., An Int. J*. **4**(5), 413-440.

C.E.N. (European Committee for Standardization). (1994), "Eurocode 1: basis of design and actions on structures. Part 2-4: Wind actions", ENV-1991-2-4, C.E.N., Brussels.

ESDU (1985), "Characteristics of atmospheric turbulence near the ground: Part 2 Single point data for strong wind - neutral atmosphere", data Item 85020, Engineering Sciences Data Unit, Lond.

Farge, M. (1992), "Wavelet transforms and their applications to turbulence", *Annu. Rev. Fluid Mech.,* **24**, 385-457.

Gurley, K. and Kareem, A. (1999), "Application of wavelet transforms in earthquake, wind and ocean engineering", *Eng. Struct.*, **21**, 149-167.

Hoxey, R.P., Richards, P.J., Richardson, G.M., Roberston, A.P., and Short, J.L. (1995), "The Silsoe Structures Building: The completed experiment part 2", In *Wind Engineering Retrospect and Prospect: Papers from the 9th International Conference,* volume III. New Age International Publishers - Wiley Easton Ltd.

Jordon, D.A., Hajj, M.R., and Tieleman, H.W. (1997), "Characterisation of turbulence scales in the atmospheric surface layer with the continuous wavelet transform", *J. Wind Eng. Ind. Aerodyn.,* **69-71**, 709-716.

Kareem, A. (1997), "Correlation structure of random pressure fields", *J. Wind Eng. Ind. Aerodyn.,* **69-71**, 507-516.

Kawai, H. (1983), "Pressure fluctuations on square prisms - applicability of strip and quasi-steady theores", *J. Wind Eng. Ind. Aerodyn.,* **13**, 197-208.

Kho, S. (2002), "Wind loadings on structures", PhD Thesis, The University of Birmingham, UK.

Kho, S, Baker, C.J., and Roberston, A. (2002), "Unsteady wind induced forces in structural members", *J. Wind Eng. Ind. Aerodyn.,* **90**, 1115-1126.

Letchford, C.W., Iverson, R.E., and McDonald, J.R. (1993), "The application of the quasi-steady theory to full-scale measurements on the Texas Tech Building", *J. Wind Eng. Ind. Aerodyn.,* **48**, 111-132.

Letchford, C.W. and Mehta, K.C. (1993), "The distribution and correlation of fluctuating pressures on the Texas Tech Building", *J. Wind Eng. Ind. Aerodyn.,* **50**, 225-234.

Letchford, C.W. and Marwood, R. (1996), "On the influence of w-component turbulence on roof pressures beneath conical vortices", Book of Abstracts - Third International Colloquium on Bluff Body Aerodynamics and Applications, VA, USA.

Newberry, C.W., Eaton, K.J., and Mayne, T.R. (1973), "Wind loading on tall buildings - further results from Royex House", Building Research Establishment Current paper 29/73 HMSO.

Prevezer, T. (1998), "Wind pressure fluctuations on a low rise building", PhD thesis, University of Nottingham, UK.

Richardson, G.M., Hoxey, R.P., Robertson, A.P., and Short, J.L. (1995), The Silsoe Structures Building: The completed experiment part 1. In *Wind Engineering Retrospect and Prospect: Papers from the 9th International Conference,* volume III. New Age International Publishers - Wiley Easton Ltd.

Richards, P.J., Fong, S., and Hoxey, R.P. (1997), "Anisotropic turbulence in the atmospheric surface layer", *J. Wind Eng. Ind. Aerodyn.,* **69-71**, 903-913.

Sharma, R.N. and Richards, P.J. (1999), "The Influence of Reynolds stresses on roof pressure fluctuations", *J. Wind Eng. Ind. Aerodyn.,* **83**, 147-157.

Standards Australia (1989), *Minimum Design Loads on Structures, Part 2: Wind loads.* Standards Australia,

North Sydney, Australian Standard AS1170.2-1989.
Torrence, C. and Compo, G.P. (1998), "A practical guide to wavelet analysis", *Bulletin of American Meteorological Society*, **79**(1), 61-78.

CC